

Condensed Matter and Interphases

Kondensirovannyye Sredy i Mezhfaznye Granitsy
<https://journals.vsu.ru/kcmf/>

Original articles

Research article

<https://doi.org/10.17308/kcmf.2021.23/3531>

TSF-MOCVD – a novel technique for chemical vapour deposition on oxide thin films and layered heterostructures

A. R. Kaul¹, R. R. Nygaard^{✉1}, V. Yu. Ratovskiy¹, A. L. Vasiliev^{2,3,4}

¹Lomonosov Moscow State University,
1 Leninskie Gory, Moscow 119991, Russian Federation

²National Research Center “Kurchatov University”,
1 pl. Akademika Kurchatova, Moscow 123182, Russian Federation

³Shubnikov Crystallography Institute of the Russian Academy of Sciences,
59 Leninskiy prospect, Moscow 119333, Russian Federation

⁴Moscow Institute of Physics and Technology,
9 Institutskiy Pereulok, Moscow Region, Dolgoprudny, 141701, Russian Federation

Abstract

A new principle for supplying volatile precursors to MOCVD gas-phase chemical deposition systems is proposed, based on a two-stage evaporation of an organic solution of precursors from a soaked cotton thread, which passes sequentially through the zones of evaporation of the solvent and precursors. The technological capabilities of TSF-MOCVD (Thread-Solution Feed MOCVD) are demonstrated based on examples of obtaining thin epitaxial films of CeO₂, h-LuFeO₃ and thin-film heterostructures β-Fe₂O₃/h-LuFeO₃. The results of studying the obtained films by X-ray diffraction, energy dispersive X-ray analysis, and high- and low-resolution transmission microscopy are presented. Using the TSF module, one can finely vary the crystallisation conditions, obtaining coatings of the required degree of crystallinity, as evidenced by the obtained dependences of the integral width of the h-LuFeO₃ reflection on the film growth rate. Based on the TEM and XRD data, it was concluded that β-Fe₂O₃ grows epitaxially over the h-LuFeO₃ layer. Thus, using TSF-MOCVD, one can flexibly change the composition of layered heterostructures and obtain highly crystalline epitaxial films with a clear interface in a continuous deposition process.

Keywords: Thread-solution feed, TSF, MOCVD, Epitaxy, Thin films, Heterostructures

Acknowledgements: the work was carried out within the framework of project No 19-33-90289 supported by Russian Foundation for Basic Research.

For citation: Kaul A. R., Nygaard R. R., Ratovskiy V. Yu., Vasiliev A. L. TSF-MOCVD – a novel technique for chemical vapour deposition on oxide thin films and layered heterostructures. *Kondensirovannyye sredy i mezhfaznye granitsy = Condensed Matter and Interphases*. 2021;23(3): 396–405. <https://doi.org/10.17308/kcmf.2021.23/3531>

Для цитирования: Кауль А. Р., Нигаард Р. Р., Ратовский В. Ю., Васильев А. Л. TSF-MOCVD – новый способ осаждения оксидных тонких пленок и слоистых гетероструктур из газовой фазы. *Конденсированные среды и межфазные границы*. 2021;23(3): 396–405. <https://doi.org/10.17308/kcmf.2021.23/3531>

✉ Roy Nygaard, e-mail: rnygaard@mail.ru

© Kaul A. R., Nygaard R. R., Ratovskiy V. Yu., Vasiliev A. L., 2021



The content is available under Creative Commons Attribution 4.0 License.

1. Introduction

Thin-film technologies underlie the development of many scientific and technical fields, and their continuous improvement gives rise to new possibilities for creating modern materials and thin-film devices with a precisely specified architecture and physical properties. Along with high-vacuum physical methods for producing thin films, chemical vapour deposition (CVD) is widely used. [1–3]. Thus, the MOC-hydride epitaxy method has taken a leading position in the production of planar semiconductor structures $A^{III}B^V$, $A^{II}B^{VI}$ and solid solutions based on them [4], and metal-organic precursor vapour deposition (MOCVD) is successfully used to obtain a wide range of oxide coatings, as well as in the development of functional materials for oxide electronics [5]. The MOCVD method started to be intensively developed at the end of the 80s of the last century due to the need to obtain thin HTSC films [6]. Over the years, this method has been demonstrated to be extremely flexible in producing films of a wide variety of compositions and purposes, as well as the ability to deposit coatings with high uniformity and over large areas. [7]. Both highly-crystalline epitaxial functional layers and heterostructures with clear interfaces with a thickness of several nanometres [8], and polycrystalline coatings with a thickness of tens of microns can be obtained using MOCVD [9].

In the deposition of multicomponent films, along with the traditional approach, which consists in the evaporation/sublimation of the precursor of each component from an individual source heated to the required temperature [7], a more convenient single source is used successfully [10, 11]. In this case, the mixture of precursors is sharply heated to a temperature providing the simultaneous transition of all precursors into a vapour, including the least volatile of them. This approach can be implemented in two ways, which differ in the aggregate states of the mixture of precursors: either an aerosol of an organic solution of a mixture of precursors [10, 11], or a fine mechanical mixture of solid precursors are used [12, 13]. Both schemes have advantages and disadvantages. For example, liquid-phase MOCVD systems are technically simpler than solid state systems and provide a continuous and smoother

feed of precursors into the reactor. However, it is important to understand that the total concentration of precursor solutions is usually in the order of 10^{-1} M, from which it follows that the vapour in the reactor is formed mainly by the organic solvent. The solvent vapour, as well as the vapour of the precursors, undergoes pyrolysis and oxidation near the substrate heated to a high temperature, which increases the concentration of residual carbon in the films, reduces and makes the partial pressure of oxygen in the deposition zone undefined [14]. It is clear that this method is of little use for the reproducible production of films of easily reducible oxides, oxides with a narrow region of oxygen homogeneity, and other films with functional properties sensitive to residual carbon.

MOCVD systems, in which the reactor is fed by the flash evaporation of micro-portions of a mixture of solid precursors, are free from these fundamental disadvantages. [12, 15], however, instead of them, there are problems with the uniformity of vapour supply to the reactor and the limited amount of precursor substances loaded into the feeder of the setup for a single experiment. The disadvantages of this approach in the implementation of the MOCVD process also include the technical complexity of setups, especially those designed specifically for the production of thin-film heterostructures. [16, 17].

This article highlights a new principle of supplying liquid precursors to chemical vapour deposition systems, which combines the advantages of known liquid-phase and solid state power supply systems and is devoid of their disadvantages [18]. Moreover, it allows obtaining thin-film structures consisting of layers of different chemical compositions within a single deposition run, as well as thin films with a vertical composition gradient.

2. Experimental

All samples were obtained using MOCVD setup with TSF module for precursor feed and a vertical hot-walled reactor. The scheme of MOCVD setup with TSF module, in which the new principle was applied, is shown in Fig. 1. During its operation, the following stages were carried out: a cotton thread (11) passed through a solution of precursors in a low-boiling solvent (6), which

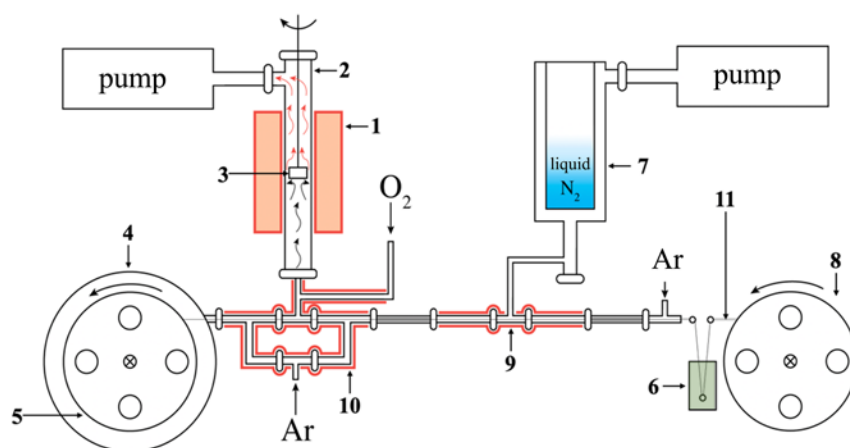


Fig. 1. The scheme of MOCVD setup with TSF module, 1 – reactor furnace, 2 – quartz reactor, 3 – substrate holder, 4 – vacuum container for the receiving reel, 5 – receiving reel, 6 – precursor reservoir, 7 – nitrogen trap, 8 – feeding reel, 9 – cold zone of the TSF module, 10 – hot zone of the TSF module, 11 – cotton thread

evaporated in the solvent distilling zone (9). After distilling off the solvent, the thread, covered with small crystals of precursors, continued to move towards the hot zone (10), where the precursors were sublimated, and the resulting vapours were transferred to the reactor (2) by heated argon flow. Directly at the inlet to the heated quartz reactor, oxygen was introduced into the gas mixture of argon with precursor vapours in a predetermined proportion. In the reactor zone, the precursor vapours decomposed in the substrate zone, which led to the formation of a thin oxide film. Throughout the entire deposition, the substrate holder (3) was rotated constantly for a more uniform heating and a more symmetrical arrangement of the substrates with respect to the gas flow directed along the normal to their surface.

During the entire deposition process, the reservoir with the precursor solution was outside the vacuum system and was accessible to the experimenter, therefore, by replacement of the solution in the reservoir (6), one could optionally change the chemical composition of the deposited oxide layers by gradual addition of additional precursors. It allowed to control the structure of the interface, making the transition between phases either abrupt or smooth, depending on the task. The proposed scheme also allowed the extremely fine variation of the film growth rate, which is an important condition for crystallisation. It can be changed by altering either the concentration of precursors in the

solution, or the speed of drawing the thread, or the absorption capacity of the thread.

The described setup was used to synthesize the following objects:

- epitaxial CeO_2 thin films on R-sapphire,
- epitaxial hexagonal LuFeO_3 (h- LuFeO_3) thin films on the (111) and (100) surfaces of YSZ single-crystal,
- thin-film heterostructures with an architecture of $\beta\text{-Fe}_2\text{O}_3(100)/\text{h-LuFeO}_3(001)/\text{YSZ}(100)$ and $\beta\text{-Fe}_2\text{O}_3(111)/\text{h-LuFeO}_3(001)/\text{YSZ}(111)$.

Metal-organic volatile complexes of $\text{Ce}(\text{thd})_4$, $\text{Lu}(\text{thd})_3$ and $\text{Fe}(\text{thd})_3$ (thd = 2,2,6,6-tetramethylheptanedionate 3,5) dissolved in toluene were used as precursors. In all cases, a temperature of 190 °C was set in the hot zone of the TSF module (10) for sublimation of the precursors. CeO_2 thin films were deposited at temperatures of 850 and 900 °C in the reactor. The total pressure in the reactor was 10 mbar and the partial pressure of oxygen in the reactor was 2, 3, 4, 5, 6, and 8 mbar. The depositions were carried out on single-crystalline r-sapphire with a surface orientation (10–12), which before deposition were annealed at a temperature of 900 °C for 30 min for the purification of the surface from the residues of adsorbed organic contaminants.

The molar ratio of precursors (Lu:Fe) in a toluene solution varied from 1 to 2 for the production of h- LuFeO_3 single-phase thin films of the required stoichiometry. It has been found that the optimal Lu:Fe ratio in the solution is 2.

h-LuFeO₃ thin films were obtained at a reactor temperature of 900 °C, a total pressure in the reactor of 10 mbar and the oxygen partial pressure in the reactor of 1 mbar. The deposition was carried out on single-crystalline YSZ [ZrO₂(Y₂O₃)] substrates with the (111) and (100) orientations of the growth surface. Before deposition, these substrates were annealed in air at a temperature of 1100 °C for 24 h, while the defects in the structure of the surface layer, damaged by the polishing of the substrates by the manufacturer, were eliminated.

Deposition of β-Fe₂O₃ layers on the h-LuFeO₃ buffer layers was carried out at a temperature in the reactor of 900 °C, the total pressure in the reactor of 10 mbar, and the partial pressure of oxygen in the reactor of 0.1 mbar.

The epitaxial growth of all films and layers was confirmed by X-ray diffraction (2θ-ω scanning) using a Rigaku Miniflex diffractometer with a copper anode (λKα = 1.54046 Å), a power of 600 W, and a beta filter. The cationic composition of h-LuFeO₃ films was determined by energy dispersive X-ray analysis using a Carl Ziess Leo SUPRA 50 VP scanning electron microscope with an X-ray system (Oxford Instruments INCA Energy+).

Cross sections of β-Fe₂O₃/h-LuFeO₃/YSZ thin-film heterostructures were prepared for transmission electron microscopy using a focused ion beam (FIB) on a Helios Nanolab 660 scanning electron microscope (ThermoFisher Scientific, USA) equipped with an Omniprobe micromanipulator (Omniprobe, USA). The cut lamellae were examined using a Titan 80-300 TEM/STEM device (FEI, USA) equipped with a C_s corrector at an accelerating voltage of 300 kV. The microscope is equipped with an EDX Si (Li) spectrometer (EDAX, USA), a high angular annular dark-field detector (HAADF) (Fischione, USA), and a Gatan Image Filter (GIF) (Gatan, USA).

3. Results and discussion

3.1. CeO₂ thin films

Epitaxial CeO₂ thin films are a very popular material with multiple applications; in particular, they are used as a buffer layer in the deposition of HTS films. CeO₂ can grow in two different orientations on R-sapphire: in one of them, the crystallographic axis [100]

is directed along the normal to the substrate plane, and in the other, the [111] axis is oriented in this direction. The [100] orientation is thermodynamically more favourable, since the R-plane of the sapphire has a rectangular motif, which promotes the growth of the cubic CeO₂ face. The growth in the [111] direction is due to kinetic reasons: as is known, this direction is the direction of the rapid growth of crystals with a fluorite structure. Our goal was to achieve the growth of films in which the fraction of (100)-oriented crystallites is maximal. The key condition for success in this case is fast surface diffusion, which promotes the crystallisation of the thermodynamically favourable (100) orientation. For acceleration of the surface diffusion, two ways were used: the first was an increase in the deposition temperature, and the second was the heterovalent doping of CeO₂ films with yttrium oxide. In the second case, diffusion is activated due to the appearance of oxygen vacancies in the growing film.

The texture coefficient (T) of the (100) orientation, calculated by equation (1), which allows estimating its share among all other orientations, taking into account the structural data was used as a quantitative characteristic of the quality of the obtained films.

$$T(100) = \frac{\frac{I_{\text{exp}}^{200}}{I_{\text{st}}^{200}} + \frac{I_{\text{exp}}^{400}}{I_{\text{st}}^{400}}}{\frac{I_{\text{exp}}^{200}}{I_{\text{st}}^{200}} + \frac{I_{\text{exp}}^{400}}{I_{\text{st}}^{400}} + \frac{I_{\text{exp}}^{111}}{I_{\text{st}}^{111}} + \frac{I_{\text{exp}}^{222}}{I_{\text{st}}^{222}}}. \quad (1)$$

For the calculation, we used the intensities of the (100) and (111) reflections in the obtained films (I_{exp}^{hkl}) determined by profile analysis of the corresponding reflections, as well as their reference intensities taken from the powder diffractogram stored in the crystallographic data base. Thus, the closer the texture coefficient is to 1, the more grains in the film are oriented with the (100) plane parallel to the substrate plane, and the more perfect is the film.

It can be seen, that the character of the texture coefficient dependence upon the oxygen partial pressure changes dramatically with an increase in temperature: at 850 °C the trend was downward (black line in Fig. 2a), while at 900 °C (black line in Fig. 2b) it changed to an upward trend.

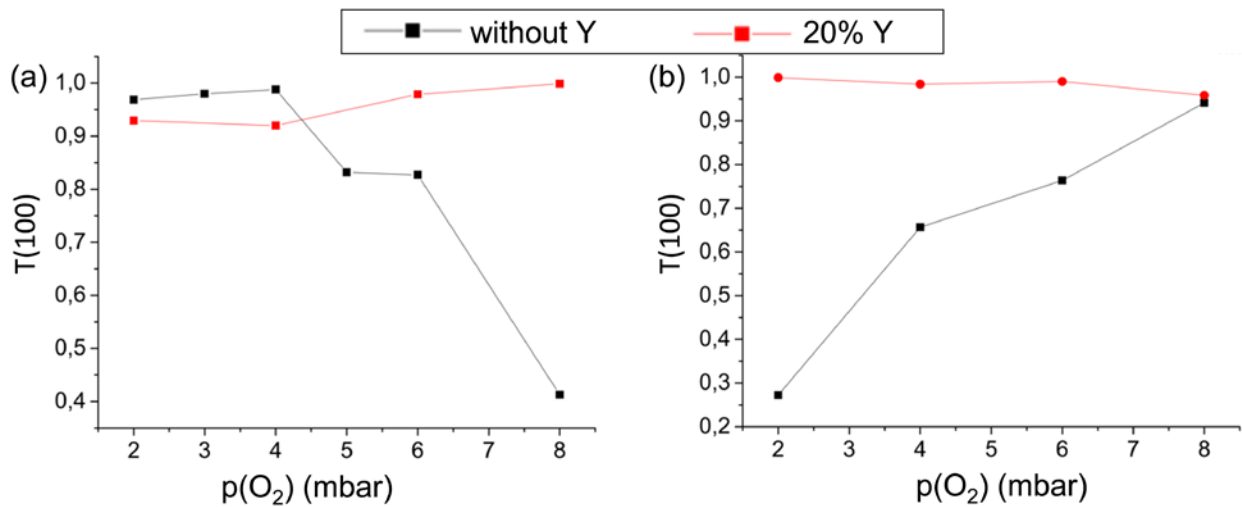
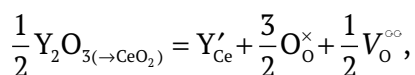


Fig. 2. Dependence of the texture orientation coefficient (100) of CeO₂ on p(O₂) and the content of the doping component (yttrium oxide) at the deposition temperature a) 850 °C and b) 900 °C

This fact can be explained as follows: at 850 °C, an increase in p(O₂) increased the deposition rate making the surface diffusion flow insufficient, which led to the formation of a larger proportion of grains with the (111) orientation. The rate of surface diffusion exponentially depends on the temperature and at a temperature of 900 °C it already becomes sufficient for the equilibrium crystallisation of the film from the substance approaching the substrate surface. However, at this temperature, the system approaches pO₂-T conditions for the dissociation of CeO₂, and phase stabilization of this oxide requires an increase in pO₂. Dissociation occurs with the formation of an equilibrium Ce₇O₁₂ [19] phase which crystallises in the rhombohedral space group R3̄c unit cell parameter $a = 6.785$ (1) Å and angle $\alpha = 99.42$ (1) [20]. The emergence of the secondary phase nuclei limits the epitaxial growth of the main CeO₂ phase in the equilibrium (100) orientation, as a result of which the (111) orientation and other polycrystalline orientations develop. This should be prevented by increasing the pO₂ in the reactor.

As we noted above, the second method for activating of surface diffusion to facilitate the achievement of the thermodynamic equilibrium is the heterovalent doping of cerium oxide with yttrium oxide, which leads to the formation of oxygen vacancies in the films:



the concentration of which is many orders of magnitude higher than the equilibrium concentration of thermal vacancies, which, in turn, leads to a sharp increase of the surface diffusion flow. As a consequence, the dependence of the texture coefficient (red line in Figs. 2a and 2b), both on the partial pressure of oxygen and on temperature, disappears, since under any deposition conditions implemented in this study, the system has sufficient diffusion mobility to reach the most energetically favourable (thermodynamically stable) variant of film growth. This result confirms the conclusions of the study [21].

3.2. *h*-LuFeO₃ thin films

Thin films of *h*-LuFeO₃ were more complex object obtained using the proposed precursor feed method. It should be noted that under the conditions of conventional solid state synthesis, LuFeO₃ crystallises with orthorhombically distorted perovskite structure [22]. Formation of the hexagonal ferrite LuFeO₃, which is isostructural to the hexagonal manganite LuMnO₃, becomes possible due to epitaxial stabilization on a structurally coherent substrate [23]. The low energy of the film – substrate interface leads to a decrease in the free energy of the system and the stabilization of phases structurally coherent to the substrate and unstable in the autonomous state [24]. In this study, YSZ(111) and YSZ(100) were used as such substrates.

For demonstration of the possibility of controlling the crystallisation conditions using the new precursor feed system, a series of depositions were carried out, varying the film growth speed by changing the thread passing speed. The X-ray diffraction results (Figs. 3a and 3b) showed that in all cases the films are h-LuFeO₃.

As can be seen from the dynamics of changes in the integral width of (002) reflection of the h-LuFeO₃ (Fig. 4), the crystallinity of the films decreased with an increase in the growth rate, which is quite a logical observation. In this case, a decrease in crystallinity can be associated not only with an insufficiently active surface diffusion flux, but also with a deviation of the system from the required stoichiometry Lu: Fe = 1: 1, leading to the formation of secondary phases enriched in iron and interfering the epitaxial growth of h-LuFeO₃. Their reflections can not be seen on the presented XRD patterns probably due to absence of the clearly defined growth direction.

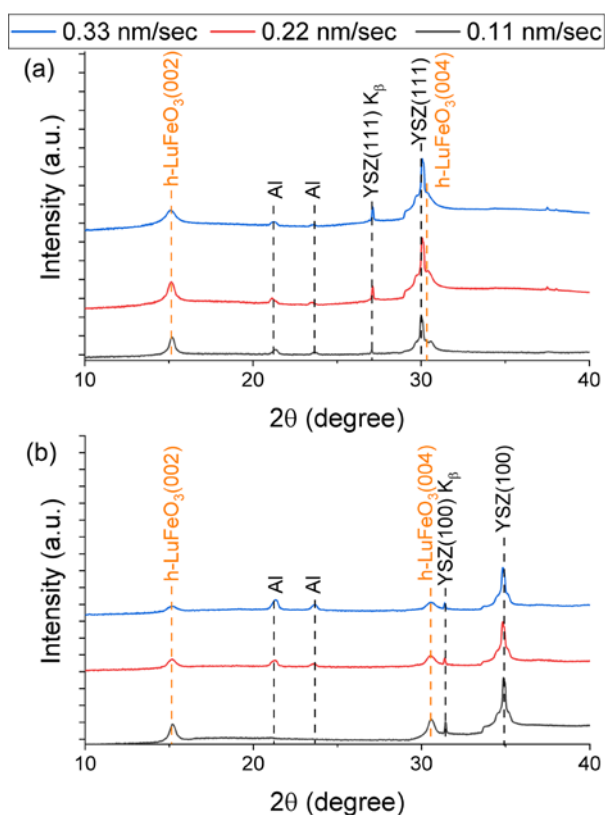


Fig. 3. Diffraction patterns of h-LuFeO₃ films obtained at different deposition rates on (a) YSZ (111) and (b) YSZ (100) substrates

An interesting feature is that the integral width of the h-LuFeO₃ reflection formed on the YSZ(100) surface in all cases was higher than that of h-LuFeO₃ on the YSZ(111) surface. The reason for this may be that the stabilizing effect of the (100) surface on h-LuFeO₃ is lower than that for the (111) surface due to the lower structural correspondence of the YSZ(100) surface to the hexagonal crystal structure of the forming film(25).

3.3. Thin-film heterostructures h-LuFeO₃+β-Fe₂O₃

The possibility of the deposition of layers of various chemical compositions was demonstrated on the example of obtaining thin-film heterostructures h-LuFeO₃ with iron oxide on single-crystalline substrates YSZ(111) and YSZ(100). It can be seen from the diffraction patterns (Fig. 5) that the iron oxide layer growing on top the h-LuFeO₃ surface is an unusual cubic modification β-Fe₂O₃. It should be noted that this phase is unstable under the implemented synthesis conditions. There is information in the literature on its transition to α-Fe₂O₃ already at 650 °C [26], while in this study, the deposition temperature of the iron oxide layer was 900 °C. The absence of phases other than β-Fe₂O₃ and the presence of only one family of reflections of this phase indicated the strong epitaxial stabilization of β-Fe₂O₃ by the h-LuFeO₃ sublayer. It should be noted that epitaxial stabilization also changes the equilibrium characteristic phase relations between Fe₂O₃ and LuFeO₃: it is well known that in mixtures of powders of this and similar systems

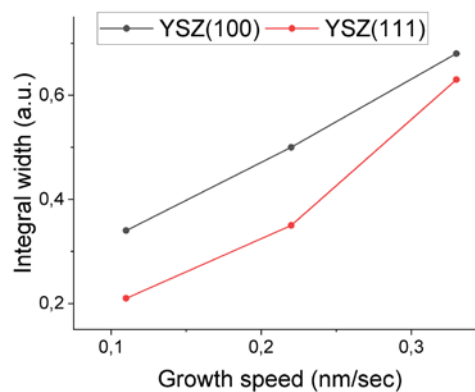


Fig. 4. Dependence of the integral width of the h-LuFeO₃ (002) reflection on the deposition rate

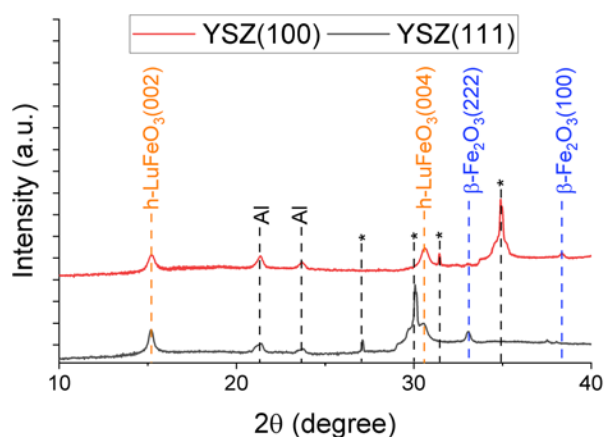


Fig. 5. Diffraction patterns of thin-film $\beta\text{-Fe}_2\text{O}_3/\text{h-LuFeO}_3$ heterostructures on YSZ (111) and YSZ (100) substrates. Reflexes of substrates are marked with *

(REE = Nd–Yb), Fe_2O_3 , and RFeO_3 REE oxides react with each other forming garnet phases [27]. However, thanks to the epitaxial contact of thin films of these substances, the chemical reaction was suppressed. Similar changes in phase relations as a result of epitaxial stabilization have been described for other oxide systems as well [24].

Also, the difference in the orientation of the epitaxially growing $\beta\text{-Fe}_2\text{O}_3$ film on YSZ surfaces with different indices should be noted: in the heterostructure deposited on the YSZ(111) substrate, the oriented growth of the $\beta\text{-Fe}_2\text{O}_3$ phase was observed in the [111] direction perpendicular to the plane of the substrate, while in the heterostructure on the YSZ(100) substrate it was observed in the [100] direction perpendicular to the plane of the substrate. The results of local electron diffraction and transmission microscopy of the cross section of the obtained heterostructures confirmed the phase composition and orientation of the layers, which were determined based on the results of X-ray diffraction. Microphotographs of $\beta\text{-Fe}_2\text{O}_3/\text{h-LuFeO}_3/\text{YSZ}$ heterostructure cross-sections (Fig. 6 a, c) indicate a higher uniformity and less surface roughness of the h-LuFeO_3 layer grown on YSZ(111) substrate compare to one deposited on YSZ(100). This observation can be explained by the previously described in-plane variant growth of h-LuFeO_3 on YSZ(100), which results in the formation of a films with microstructure fragmented into nanoscale domains [25]. The

closer examination of images of heterostructure $\beta\text{-Fe}_2\text{O}_3(001)/\text{h-LuFeO}_3(001)/\text{YSZ}(100)$ revealed that h-LuFeO_3 had not formed located uniformly in one direction: its (001) planes were aligned parallel to both (001) and (111) planes of the YSZ substrate. The former growth variant is observed near the substrate surface and continues up to film thickness of roughly 25 nm where the growth direction is switched to the later variant. The presence of the side orientation of h-LuFeO_3 in the YSZ(100) heterostructure is very interesting and can be a factor explaining the difference in the growth direction of the $\beta\text{-Fe}_2\text{O}_3$ on different substrates. Thus, in the heterostructure on YSZ(111) substrate the stabilizing surface for $\beta\text{-Fe}_2\text{O}_3$ is h-LuFeO_3 with its (001) plane parallel to the substrate plane while in case of YSZ(100) substrate $\beta\text{-Fe}_2\text{O}_3$ is stabilized on h-LuFeO_3 with its (001) plane inclined by 54.7° relative to the substrate plane (54.7° is the angle between $\langle 111 \rangle$ and $\langle 100 \rangle$ directions in the cubic cell). This substantiation of the $\beta\text{-Fe}_2\text{O}_3$ growth is also reinforced by the fact that the angle between the crystallographic directions of $\beta\text{-Fe}_2\text{O}_3$ in heterostructures on different substrates ($\langle 111 \rangle$ on YSZ(111) and $\langle 100 \rangle$ on YSZ(100)) is also 54.7° .

Grains of $\beta\text{-Fe}_2\text{O}_3$ with clearly visible grain boundaries are clearly seen on microphotographs of heterostructures deposited on both substrates, which indicates Volmer–Weber type (island) growth. The growth of iron oxide layer with a thickness of about 5 nm on the surface of the $\beta\text{-Fe}_2\text{O}_3$ in the heterostructure on the YSZ(111) substrate should be noted (Fig. 6b). According to the Fourier spectrum, this nanolayer can be described by a cubic syngony with a lattice parameter of 8.4 Å, which can correspond to the Fe_3O_4 phase with a lattice parameter of 8.396 nm (ICDD PDF-2 database). Its appearance in this heterostructure and, on the contrary, its absence in the heterostructure on the YSZ(100) substrate (Fig. 6c, d) can be explained by the fact that, in the former case, the critical thickness of the $\beta\text{-Fe}_2\text{O}_3$ film is exceeded, above which the energy lowering of $\beta\text{-Fe}_2\text{O}_3(111)/\text{h-LuFeO}_3(001)$ epitaxial contact turns out to be insufficient to stabilize this metastable modification of iron oxide. At the same time, in the heterostructure on the YSZ(100) substrate, $\beta\text{-Fe}_2\text{O}_3$ grows in a different orientation relative to h-LuFeO_3 , which obviously

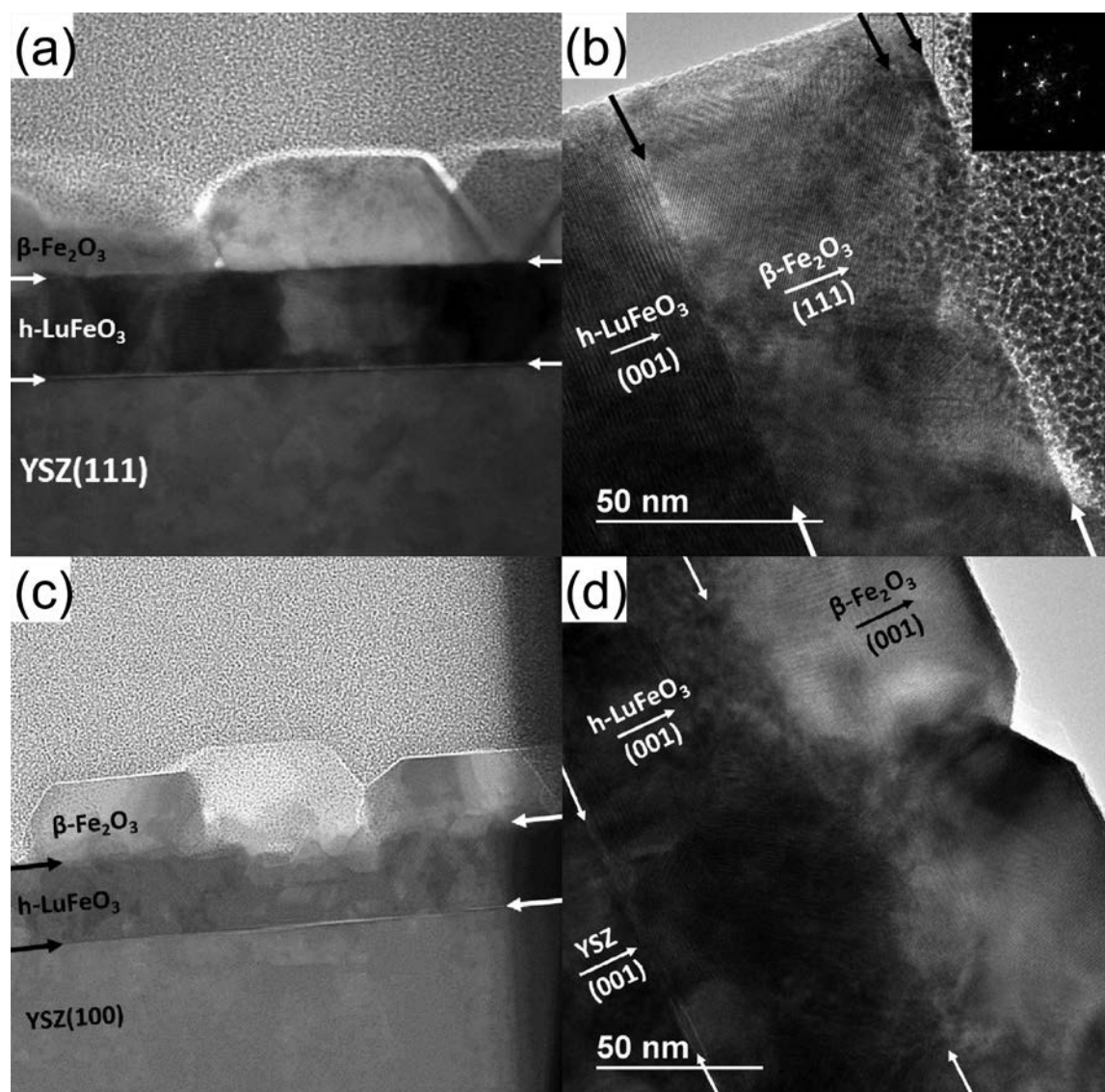


Fig. 6. Results of cross-section TEM of heterostructures (a, b) $\beta\text{-Fe}_2\text{O}_3$ (111)/ h-LuFeO_3 (001)/YSZ (111) and (c, d) $\beta\text{-Fe}_2\text{O}_3$ (001)/ h-LuFeO_3 (001)/YSZ (100)

leads to an increase in the critical thickness of this epitaxially stabilized layer. This interesting aspect, the dependence of the critical thickness on the orientation of epitaxially stabilized phase, will be clarified by further calculations of the interface energies using the algorithm described by us in [25].

4. Conclusions

Thus, we have implemented a new version of the MOCVD with an original method for supplying volatile precursors to the reactor, called TSD-MOCVD, which combines the advantages of liquid-phase and solid-state single-source MOCVD variants. The deposition

occurs at a low total pressure in the reactor, the precursor solution is available to the operator throughout the experiment, which allows one to change the composition of the solution and/or its concentration, make a cyclic change, and to add new components to it. The new method was used for the deposition of CeO_2 films, the possibility of a smooth change in the deposition rate, its effect, as well as the effect of heterovalent doping on the texture of the films are shown. The great preparative capabilities of the proposed method for the growth of epitaxial heterostructures with a clear interface were based on the examples of $\beta\text{-Fe}_2\text{O}_3(111)/\text{h-LuFeO}_3(001)/\text{YSZ}(111)$ and $\beta\text{-Fe}_2\text{O}_3(001)/\text{h-LuFeO}_3(001)/\text{YSZ}(100)$.

LuFeO₃(001)//YSZ(100). The possibility of the epitaxy of metastable β-Fe₂O₃ polymorph on the surface of hexagonal lutetium ferrite was revealed for the first time. The existence of both phases is explained within the framework of the phenomenon of epitaxial stabilization. Such film composites will be further investigated for possible multiferroic properties.

Author contributions

Kaul A. R. – scientific leadership, research concept, text writing. Nigaard R. R. and Ratovskiy V. Yu. – conducting experiments on gas-phase deposition of thin films and heterostructures, processing the results of X-ray diffraction and transmission electron microscopy, text writing. Vasiliev A. L. – carrying out transmission electron microscopy and discussion of its results.

Conflict of interests

The authors declare that they have no known competing financial interests or personal relationships that could have influenced the work reported in this paper.

References

1. Blocher J. Coating by chemical vapor deposition (CVD). *SAE Technical Paper Series*. 1973;82: 1780–6. <https://doi.org/10.4271/730543>
2. Pierson H. *Handbook of chemical vapor deposition*. 2nd ed. Noyes Publications; 1999. 506 p. <https://doi.org/10.1016/B978-081551432-9.50005-X>
3. Syrkin V. G. CVD- metod. *Khimicheskaya parofaznaya metallizatsiya* [CVD-method of chemical vapor-phase metallization]. Nauka Publ.; 2000. 495 p. (In Russ.)
4. Akchurin R. H., Marmalyuk A. A. *MOS-gidridnaya epitaksiya v tekhnologii materialov fotoniki i elektroniki* [MOC-hybrid epitaxy in the technology of materials for photonics and electronics]. Technosphaera Publ.; 2018. 488 p. (In Russ.)
5. Wright P. J., Crosbie M. J., Lane P. A., Williams D. J., Jones A. C., Leedham T. J., Davies H. O. Metal organic chemical vapor deposition (MOCVD) of oxides and ferroelectric materials. *Journal of Materials Science: Materials in Electronics*. 2002;13(11): 671–678. <https://doi.org/10.1023/a:1020618411750>
6. Wahl G., Arndt J., Stadel O. Chemical vapor deposition of superconductor and oxide films. In: *Chemical physics of thin film deposition processes for micro- and nano-technologies*. Springer; 2002. p. 145–170. https://doi.org/10.1007/978-94-010-0353-7_7
7. Choy K. L. Chemical vapour deposition of coatings. *Progress in Materials Science*. 2003;48(2): 57–170. [https://doi.org/10.1016/s0079-6425\(01\)00009-3](https://doi.org/10.1016/s0079-6425(01)00009-3)
8. Dubourdieu C., Rosina M., Audier M., Weiss F., Sénateur J. P., Dooryhee E., Hodeau J. L. Application of pulsed liquid-injection MOCVD to the growth of ultrathin epitaxial oxides for magnetic heterostructures. *Thin Solid Films*. 2001;400(1–2): 81–84. [https://doi.org/10.1016/s0040-6090\(01\)01457-2](https://doi.org/10.1016/s0040-6090(01)01457-2)
9. Samoilenkov S. V., Stefan M. A., Wahl G. MOCVD of thick YSZ coatings using acetylacetonates. *Surface and Coatings Technology*. 2005;192(1): 117–123. <https://doi.org/10.1016/j.surfcoat.2004.03.019>
10. Weiss F., Audier M., Bartaszyte A., Bellet D., Girardot C., Jimenez C., ... Ternon C. Multifunctional oxide nanostructures by metal-organic chemical vapor deposition (MOCVD). *Pure and Applied Chemistry*. 2009;81(8): 1523–1534. <https://doi.org/10.1351/pac-con-08-08-10>
11. Sénateur J.-P., Dubourdieu C., Galindo V., Weiss F., Abrutis A. Application of pulsed injection MOCVD to the deposition of oxide single layers and superlattices. In: *Innovative processing of films and nanocrystalline powders*. 2002. p. 71–105. https://doi.org/10.1142/9781860949623_0003
12. Kartavtseva M. S., Gorbenko O. Y., Kaul A. R., Akbashev A. R., Murzina T. V., Fusil S., Barthélémy A., Pailloux F. BiFeO₃ thin films prepared by MOCVD. *Surface and Coatings Technology*. 2007;201(22–23): 9149–9153. <https://doi.org/10.1016/j.surfcoat.2007.04.099>
13. Bibes M., Gorbenko O., Martínez B., Kaul A., Fontcuberta J. Alkaline-doped manganese perovskite thin films grown by MOCVD. *Journal of Magnetism and Magnetic Materials*. 2000;211(1–3): 47–53. [https://doi.org/10.1016/s0304-8853\(99\)00712-x](https://doi.org/10.1016/s0304-8853(99)00712-x)
14. Decker W., Erokhin Y., Gorbenko O., Graboy I., Kaul A., Nurnberg A., Pulver M., Stolle R., Wahl G.. Low-pressure single aerosol source MOCVD of YBCO thin films. *Journal of Alloys and Compounds*. 1993;195(C): 291–294. [https://doi.org/10.1016/0925-8388\(93\)90742-6](https://doi.org/10.1016/0925-8388(93)90742-6)
15. Kaul A. R., Seleznev B. V. New principle of feeding for flash evaporation MOCVD devices. *Le Journal de Physique IV*. 1993;3(3): 375–378. <https://doi.org/10.1051/jp4:1993351>
16. Menushenkov A. P., Ivanov V. G., Chepikov V. N., Nygaard R., Soldatenko A., Rudnev I. A., ... Monteseuro V. Correlation of local structure peculiarities and critical current density of 2G MOCVD YBCO tapes with BaZrO₃ nano-inclusions. *Superconductor Science and Technology*. 2017;30(4): 045003. <https://doi.org/10.1088/1361-6668/aa599c>
17. Shukin A. E., Kaul A. R., Vasiliev A. L., Rudnev I. A. Synthesis, structure and superconducting

properties of laminated thin film composites $\text{YBa}_2\text{Cu}_3\text{O}_{7-\delta}/\text{Y}_2\text{O}_3$ as the components of 2G HTS tapes. *Kondensirovannye sredy i mezhfaznye granitsy = Condensed Matter and Interphases*. 2021;23(1): 122–139. <https://doi.org/10.17308/kcmf.2021.23/3313>

18. Kaul A. R., Seleznev B. V., Sharovarov D. I., Nygaard R. R., Osipova Yu. A., Makarevich A. M., Sadykov I. I. Feeding system for supplying volatile compounds in reactors of chemical vapor-phase deposition: *Patent No 2722914 RF*. Claim. 03.12.2019. Publ. 04.06.2020. Byul. No 2019139340.

19. Niu G., Zoellner M. H., Schroeder T., Schaefer A., Jhang J. H., Zielasek V., ... Reichling M. Controlling the physics and chemistry of binary and ternary praseodymium and cerium oxide systems. *Physical Chemistry Chemical Physics*. 2015;17(38): 24513–2540. <https://doi.org/10.1039/c5cp02283e>

20. Kummerle E. A., Heger G. The structures of $\text{C-Ce}_2\text{O}_{3+8}$, Ce_7O_{12} , and $\text{Ce}_{11}\text{O}_{20}$. *Journal of Solid State Chemistry*. 1999;147(2): 485–500. <https://doi.org/10.1006/jssc.1999.8403>

21. Hayes W., Stoneham A. M. Defects and defect processes in nonmetallic solids. New York: John Wiley & Sons; 2004. 472 p.

22. Chowdhury U., Goswami S., Bhattacharya D., Rajput S. S., Mall A. K., Garg A., ... Bhattacharya D. Origin of ferroelectricity in orthorhombic LuFeO_3 . *Physical Review B*. 2017;100(19): 1–5. <https://doi.org/10.1103/physrevb.100.195116>

23. Bossak A., Graboy I., Gorbenko O., Kaul A., Kartavtseva M., Svetchnikov V., Zandbergen H. W. XRD and HREM studies of epitaxially stabilized hexagonal orthoferrites RFeO_3 (R = Eu-Lu). *Chemistry of Materials*. 2004;16(9): 1751–1755. <https://doi.org/10.1021/cm0353660>

24. Kaul A. R., Gorbenko O. Yu., Kamenev A. A. The role of heteroepitaxy in the development of new thin-film oxide-based functional materials. *Russian Chemical Reviews*. 2004;73(9): 861–880. <https://doi.org/10.1070/rc2004v073n09abeh000919>

25. Markelova M., Nygaard R., Tsybarenko D., Shurkina A., Abramov A., Amelichev V., ... Kaul A.

Multiferroic h- LuFeO_3 thin films on (111) and (100) surfaces of YSZ substrates: An experimental and theoretical study. *ACS Applied Electronic Materials*. 2021;3(2): 1015–1022. <https://doi.org/10.1021/acsaelm.0c01127>

26. Zboril R., Mashlan M., Krausova D., Pikal P. Cubic $\beta\text{-Fe}_2\text{O}_3$ as the product of the thermal decomposition of $\text{Fe}_2(\text{SO}_4)_3$. *Hyperfine Interact.* 1999;120–121(1–8): 497–501. <https://doi.org/10.1023/a:1017018111071>

27. Manimuthu P., Manikandan M., Selvi M. M., Venkateswaran C. Multiferroic $\text{Lu}_3\text{Fe}_5\text{O}_{12}$ for magneto-dielectric applications. *AIP Conference Proceedings*. 2012;1447(1): 1205–1206. <https://doi.org/10.1063/1.4710443>

Information about the authors

Andrey R. Kaul, DSc in Chemistry, Full Professor at the Chair of Inorganic Chemistry, Lomonosov Moscow State University, Moscow, Russian Federation; arkaul@mail.ru. ORCID iD: <https://orcid.org/0000-0002-3582-3467>.

Roy R. Nygaard, Junior Research Fellow at the Chair of Inorganic Chemistry, Lomonosov Moscow State University, Moscow, Russian Federation; e-mail: rnygaard@mail.ru. ORCID iD:

Vadim Yu. Ratovskiy, student at the Higher School of Material Science, Lomonosov Moscow State University, Moscow, Russian Federation; e-mail: vratovskiy@bk.ru. ORCID iD: <https://orcid.org/0000-0003-1657-110X>.

Alexander L. Vasiliev, PhD in Physics and Mathematics, Associate Professor at the Faculty of NBICS, Moscow Institute of Physics and Technology, Moscow, Russian Federation; email: a.vasiliev56@gmail.com. ORCID iD: <https://orcid.org/0000-0001-7884-4180>.

Received 1 July 2021; Approved after reviewing 15 July 2021; Accepted for publication 15 August 2021; Published online 25 September 2021.

*Translated by Valentina Mittova
Edited and proofread by Simon Cox*